

Safety-Critical Formation Control of Non-Holonomic Multi-Robot Systems in Communication-Limited Environments

Vishrut Bohara and Siavash Farzan

Abstract—This paper presents a robust estimator-based safety-critical controller for formation control of non-holonomic mobile robots in communication-limited environments. The proposed decentralized framework integrates a robust state estimator with a formation tracking control law that guarantees inter-agent collision avoidance using control barrier functions. String stability is incorporated into the control design to maintain stability against noise from predecessors in leader-follower formations. Rigorous stability analysis using Lyapunov functions ensures the stability of estimation errors and the convergence of the formation to desired configurations. The effectiveness and robustness of the proposed approach are validated through numerical simulations of various maneuvers and realistic Gazebo experiments involving formations in a warehouse environment. The results demonstrate the controller’s ability to maintain safety, achieve precise formation control, and mitigate disturbances in scenarios without inter-robot communication.

I. INTRODUCTION

Multi-robot systems are emerging as a transformative technology in robotics due to their potential for increased productivity, scalability, coverage, and cost-effectiveness compared to single-robot systems. Their coordinated actions open up possibilities for complex tasks in areas like environmental monitoring, industrial automation, and disaster response [1]. A key challenge in realizing this potential is formation control – the ability of multiple robots to maintain desired spatial arrangements while performing both individual and collaborative tasks. In many real-world scenarios, communication between robots is constrained or unreliable, and sensor data may be noisy or incomplete, creating a need for robust, safe, and decentralized formation control strategies. These information-limited environments are often found in safety-critical applications, where failures can have severe consequences. Examples include search and rescue missions in disaster areas, infrastructure inspections in hazardous conditions, or coordinated operations in environments with communication jamming. Developing formation control strategies that guarantee safety and stability in such environments is therefore of paramount importance. This research addresses this challenge by proposing a novel approach that combines estimation and control techniques to achieve safe and reliable formation control in communication-limited scenarios.

Various control schemes for formation control have been proposed, addressing challenges like inter-agent safety, stability, and operation in communication-constrained environments (see the survey in [2]). Researchers have tackled various subsets of the challenges associated with formation control. Some approaches, like in [3], utilize observer-based controllers and differentiators to achieve formation tracking in quadrotors, even with inaccessible linear velocity measurements and unknown disturbances. Others, such as [4], incorporate trajectory estimation using techniques like Extended Kalman Filters to achieve formation control without explicit communication, though often lacking rigorous stability guarantees. The work in [5] addresses formation control for mobile robots with limited communication using distributed estimation, achieving asymptotic stability. However, it doesn’t extend to scenarios with no communication. Similarly, while studies like [6] and [7] explore estimation-based control strategies with bearing measurements or in the absence of relative orientation, they don’t fully address the challenges of safety-critical applications in information-limited settings. The collective findings from these studies underscore the potential of estimation-based control for formation control in communication-constrained environments. However, a critical gap remains in addressing safety-critical scenarios with stringent requirements for stability, robustness, and collision avoidance.

Recent advances in control barrier functions (CBFs) for safety assurance [8] have sparked significant interest in the development of safety-critical systems, particularly those focused on preventing collisions between agents and with the environment. For instance, the authors in [9] utilize high-order CBFs to ensure safety in formation control, assuming local communication for the sharing of position and velocity data between neighboring agents. In a similar vein, the work presented in [10] introduces a displacement-based formation control approach that maintains safety through a controller design incorporating artificial potential functions and CBFs. However, this method lacks a stability analysis for velocity tracking and lacks evaluation in realistic simulation environments. Other notable research directions include the integration of CBFs with reinforcement learning [11] and model predictive control strategies [12] to achieve safe formation control.

Formation reconfiguration in heterogeneous swarms, as presented in [13], and obstacle avoidance via reconfiguration in [14], further highlight the diverse challenges in formation control. While these works address important aspects of this complex domain, they do not explicitly focus on ensuring safety

Vishrut Bohara is with the Robotics Engineering Department, Worcester Polytechnic Institute, Worcester, MA 01609, USA (e-mail: vbohara@wpi.edu).

Siavash Farzan is with the Electrical Engineering Department, California Polytechnic State University, San Luis Obispo, CA 93407, USA (e-mail: sfarzan@calpoly.edu).

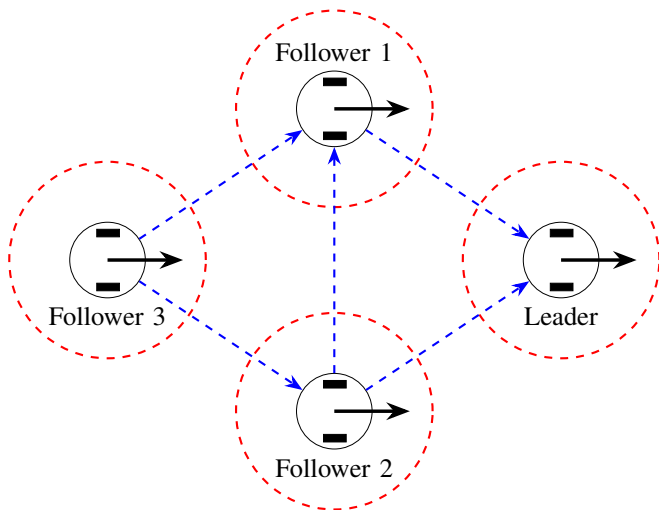


Fig. 1. Leader-Follower formation control of mobile robots in a diamond formation, illustrating inter-agent interaction edges and safety boundaries. The red dashed circles denote the safety regions for each robot, and the blue dashed arrows represent predecessor-follower interactions, where followers maintain desired distances from their predecessors without communication.

within the formation. The authors of [15] have identified the need for a unified system that achieves both stability and safety using CBF and Lyapunov functions. However, their work does not focus on the challenges of operating in communication-limited environments or provide validation in physics-realistic environments.

Contributions focusing on formation control without communication include the velocity observer for non-holonomic mobile agents, and the state feedback controller presented in [16]. The distributed observer approach in [17] enables leader-following control in multi-agent networks without explicit communication. Furthermore, robust time-varying controller designs with extended state observers for second-order multi-agent systems are explored in [18]. A related study in [19] utilizes an estimator-based controller to achieve safety and stability in adaptive cruise control, which can be seen as a one-dimensional form of formation control.

In summary, existing literature on formation control lacks a unified framework that proves stability, guarantees safety, operates in a communication-limited environment, and works with robots with non-holonomic constraints. This research addresses this gap by introducing an estimator-based safety-critical controller for the formation control of mobile robots in communication-limited environments. The main contributions of this research include:

- i) a robust estimator design for non-holonomic robot swarms, accompanied by a rigorous stability proof;
- ii) a decentralized formation control algorithm with provable guarantees of inter-agent collision avoidance;
- iii) the introduction of string stability as a critical metric for leader-follower formation control, ensuring disturbance attenuation throughout the formation; and
- iv) extensive numerical simulations and Gazebo-based experiments to validate the effectiveness and robustness of the proposed estimator and controller in realistic scenarios.

This paper is organized as follows. Section II formally

describes the problem of safety-critical leader-following formation control and the underlying system dynamics. Section III presents our proposed estimator-based safety-critical controller, including its design, stability analysis, and integration with the control law. Section IV evaluates the performance of the proposed approach through numerical simulations and physics engine-based Gazebo experiments. Finally, Section V concludes the paper and outlines potential avenues for future research.

II. PROBLEM DESCRIPTION

Safety-critical leader-following formation control involves coordinating multiple robots to achieve and maintain a desired spatial arrangement while ensuring collision avoidance. In information-limited environments, where communication is constrained and sensor data may be noisy or incomplete, ensuring safety poses a significant challenge.

This work addresses a specific sub-problem within leader-following formation control characterized by the following conditions: each robot perceives only its velocity and the relative distances to other agents, with no communication between robots. Agents maintain non-negative linear velocities. All agents are equipped with sensors that detect both the radial and angular positions of other agents. Importantly, the center of rotation of the leader's trajectory must remain outside the formation to ensure achievable control.

We propose an estimator-based safety-critical framework to solve this problem, guaranteeing string stability, estimator stability, and inter-agent safety. While focusing on the leader-follower model (one of the most safety-critical), our approach can be extended to fully decentralized multi-agent systems. The estimator design remains applicable across various 2D applications, offering a foundation for safe, decentralized control.

A. Predecessor-Follower Dynamics

In a leader-follower formation, we model the motion of a robot pair using predecessor-follower dynamics. Consider the i^{th} robot following the $(i-1)^{th}$ robot. We define the following in the follower's frame of reference (see Fig. 2).

State Variables: The state of the system is characterized by several variables. These include the distance between the robots (d), the angular position of the predecessor relative to the follower's heading (θ), the linear velocities of both the predecessor and follower (v_1 and v respectively) and the angle between the predecessor's heading and the follower's x-axis, i.e. follower's heading (ψ). From these states, the observable states for followers are d, θ, v .

Control Inputs: The control inputs in the dynamics are the linear accelerations of the predecessor and follower (u_1 and u respectively). The angular velocities of both robots (ω_1 and ω) also serve as control inputs, influencing the heading of the agent. The desired control law is expected to calculate u and ω to maintain the desired distance from the predecessor.

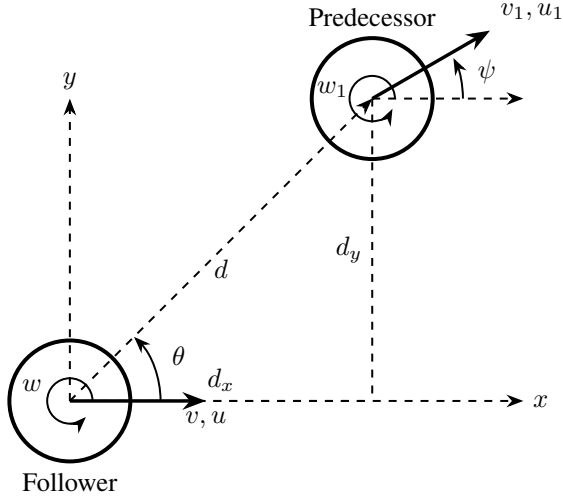


Fig. 2. Predecessor-follower pair and associated parameters in a leader-follower formation control setting.

System Dynamics: The system's evolution is described by the following equations:

$$\begin{aligned} \dot{d} &= v_1 \cos(\theta - \psi) - v \cos \theta \\ \dot{\theta} &= \frac{v \sin \theta - v_1 \sin(\theta - \psi)}{d} - \omega \\ \dot{v}_1 &= u_1 \\ \dot{v} &= u \\ \dot{\psi} &= \omega_1 - \omega \end{aligned} \quad (1)$$

We can project these dynamics onto the follower's frame of reference:

$$\begin{aligned} \dot{d}_x &= v_1 \cos \psi - v + d \omega \sin \theta = v_{1x} - v + d_y \omega \\ \dot{d}_y &= v_1 \sin \psi - d \omega \cos \theta = v_{1y} - d_x \omega \\ \dot{v}_{1x} &= u_1 \cos \psi - v_{1y} (\omega_1 - \omega) = a_x + v_{1y} \omega \\ \dot{v}_{1y} &= u_1 \sin \psi + v_{1x} (\omega_1 - \omega) = a_y - v_{1x} \omega \end{aligned} \quad (2)$$

Constraints: The movements of the robots are subject to physical constraints. The follower's linear velocity (v) must remain between zero and a maximum value (v_{max}). The magnitudes of linear accelerations (u_1 and u) are bounded by a maximum acceleration (u_{max}). Similarly, there's a maximum angular velocity (ω_{max}). These individual constraints also lead to a combined bound on the components of the predecessor's acceleration in the follower's frame of reference ($|a_x|$, $|a_y|$). These constraints can be summarized as:

$$\begin{aligned} 0 \leq v \leq v_{max}, \quad |u| \leq u_{max}, \quad |\omega| \leq \omega_{max} \\ |a_x|, |a_y| \leq u_{max} + v_{max} \omega_{max} = a_{max} \end{aligned} \quad (3)$$

B. Formation Control

In this framework, we represent the formation of one leader and n follower agents as a directed acyclic graph (DAG). Here's how the graph formalizes the leader-follower relationships:

- i. Nodes: A node in the graph represents each agent (leader and followers).
- ii. Edges: An edge represents a predecessor-follower interaction, with the predecessor at the head of the edge and the

follower at the tail. An interaction is defined as a follower sensing the distance and angular position of the predecessor in a local coordinate frame using onboard sensors. Each edge is designated as either an X^+ -edge or a Y -edge: an X^+ -edge is when a velocity-dependent distance is maintained from the predecessor along the follower's X-axis. A Y -edge is when a fixed distance is maintained from the predecessor along the follower's Y-axis.

iii. Graph Constraints: Every follower (except the first) must have at least one X^+ -edge and one Y -edge. For each follower (except the first), the predecessors associated with the X^+ -edge and Y -edge must be different. The first follower's X^+ - and Y -edges both point to the leader.

Fig. 1 illustrates a diamond formation with four nodes (one leader, three followers). This formation's DAG has the following edges: three X^+ -edges ($F_1 \rightarrow L$, $F_2 \rightarrow L$, $F_3 \rightarrow F_2$), and three Y -edges ($F_1 \rightarrow L$, $F_2 \rightarrow F_1$, $F_3 \rightarrow F_1$), where L is the leader and F_1 , F_2 , F_3 are the followers.

C. String Stability

String stability [20] is a crucial metric in leader-follower formations, particularly in safety-critical scenarios. It signifies a follower's capacity to both attenuate disturbances originating from the leader's motion and maintain a safe distance. Formally, string stability is quantified using the string stability gain (\mathcal{S}), which compares the amplitude of a disturbance in the leader to the corresponding disturbance experienced by the follower. A formation is string stable if $\mathcal{S} < 1$, meaning disturbances are attenuated as they propagate through the chain of followers.

For a multi-agent formation to be considered stable, it must meet the string stability criteria described above and maintain safe inter-agent distances. The distance between each predecessor-follower pair must remain within a predefined safe range (a minimum distance to prevent collisions and a maximum distance to maintain formation integrity).

In the following section, we will leverage Lyapunov functions and Control Barrier Functions (CBF) alongside these stability definitions to design an estimator-based controller that guarantees safety and achieves the desired string stability with formation tracking.

III. ESTIMATOR-BASED SAFETY CRITICAL CONTROLLER

In a formation control setup without communication, each agent needs accurate estimates of other agents' velocities to achieve optimal control. This section presents the design of a stable estimator, explores its stability analysis, and outlines the integration of this estimator into a safety-critical controller.

A. Estimator Design

To begin, let's define the notation used in our estimator design. We represent the estimates of the system states d_x , v_{1x} , d_y , v_{1y} as \hat{d}_x , \hat{v}_{1x} , \hat{d}_y , \hat{v}_{1y} , respectively. The differences between the true states and their corresponding estimates are the estimation errors, denoted by \tilde{d}_x , \tilde{v}_{1x} , \tilde{d}_y , \tilde{v}_{1y} . Finally, the constant gains g_d , g_v , and p are used to tune the estimator's performance.

Assuming an agent has access to its distance from its predecessor (d), the angular position of the predecessor relative to its own heading (θ), its own linear velocity (v), and its own angular velocity (ω), the estimator is designed as follows:

$$\begin{aligned}\dot{\tilde{d}}_x &= \hat{v}_{1x} - v + d\omega \sin\theta + g_d \tilde{d}_x \\ \hat{v}_{1x} &= g_v \tilde{d}_x + \hat{v}_{1y} \omega + p\omega \tilde{d}_y \\ \dot{\tilde{d}}_y &= \hat{v}_{1y} - d\omega \cos\theta + g_d \tilde{d}_y \\ \hat{v}_{1y} &= g_v \tilde{d}_y - \hat{v}_{1x} \omega - p\omega \tilde{d}_x\end{aligned}\quad (4)$$

Given the velocity estimates are accurate, the heading and velocity of the predecessor can be calculated as:

$$\begin{aligned}\hat{\psi} &= \tan^{-1} \frac{v_{1y}}{v_{1x}} \\ \hat{v}_1 &= \sqrt{\hat{v}_{1x}^2 + \hat{v}_{1y}^2}\end{aligned}\quad (5)$$

To analyze the estimator's stability, we need to examine the dynamics of the estimation error. Let $\tilde{e} = [\tilde{d}_x, \tilde{v}_{1x}, \tilde{d}_y, \tilde{v}_{1y}]^T$ represent the error vector. The estimation error dynamics can then be expressed using (2,4) as:

$$\dot{\tilde{e}} = \begin{bmatrix} g_d & 1 & 0 & 0 \\ g_v & 0 & p\omega & \omega \\ 0 & 0 & g_d & 1 \\ -p\omega & -\omega & g_v & 0 \end{bmatrix} \tilde{e} + \begin{bmatrix} 0 & 0 \\ -1 & 0 \\ 0 & 0 \\ 0 & -1 \end{bmatrix} \begin{bmatrix} a_x \\ a_y \end{bmatrix} = A\tilde{e} + Ba_e\quad (6)$$

This formulation of the estimation error dynamics allows us to systematically analyze the estimator's stability properties in the following subsection.

B. Stability Analysis

To guarantee the estimator dynamics' accuracy, we analyze its stability under three key scenarios using Lyapunov function candidates. First, we consider the case where the predecessor vehicle maintains a constant linear velocity and zero angular velocity. This analysis provides insights into the estimator's behavior under ideal conditions and establishes a baseline for our stability considerations. Next, we examine a more complex scenario where the predecessor's linear velocity can vary over time, but its angular velocity (ω_1) and follower's angular velocity (ω) remain zero. Demonstrating the estimator's global boundedness, in this case, ensures its robustness in the face of more realistic motion patterns. Finally, we extend the analysis to the most general scenario where the predecessor exhibits both time-varying linear and non-zero angular velocity. By proving the estimator maintains global boundedness here, we establish that it can reliably adapt to complex and dynamic scenarios. The stability analysis for Case 1 is outlined as follows.

Case 1: Constant velocity

Consider a Lyapunov function candidate of the form: $V_1 = \tilde{e}^T P \tilde{e}$, where $P = P^T > 0$ is a positive definite matrix. To ensure system stability, we need to find a matrix P that satisfies the continuous algebraic Riccati equation: $A^T P + P A + Q = 0$ [21] where A is defined in (III-A), and $Q = Q^T > 0$ is a positive definite matrix.

Lemma 1. *For a Hurwitz matrix A and a positive definite matrix Q , there exists a unique positive definite matrix P such that $A^T P + P A + Q = 0$ [21].*

Lemma 1 implies that if the state matrix A is Hurwitz (all eigenvalues have negative real parts), the Lyapunov function candidate V_1 guarantees stability. This requirement necessitates constraints on estimator gains, which are calculated using the determinant characteristic equation of the state matrix A as follows:

$$\omega^2(\lambda - g_d + p)^2 + (\lambda^2 - g_d \lambda - g_v)^2 = 0\quad (7)$$

For all roots of (7) to have negative real parts, the following bounds on the estimator gains must be satisfied:

$$g_d < 0, \quad \frac{-g_d^2}{4} \leq g_v < 0\quad (8)$$

$$p = \frac{1}{2} \left(g_d + \sqrt{g_d^2 + 4g_v} \right)\quad (9)$$

Case 2: Time-varying linear velocity with $\omega = \omega_1 = 0$

In this scenario, the estimator dynamics is as follows:

$$\dot{\tilde{e}} = \begin{bmatrix} g_d & 1 & 0 & 0 \\ g_v & 0 & 0 & 0 \\ 0 & 0 & g_d & 1 \\ 0 & 0 & g_v & 0 \end{bmatrix} \tilde{e} + \begin{bmatrix} 0 & 0 \\ -1 & 0 \\ 0 & 0 \\ 0 & -1 \end{bmatrix} a_e\quad (10)$$

For the stability analysis, we choose the following Lyapunov candidate function:

$$V = \frac{1}{2} ((r\tilde{d}_x - \tilde{v}_x)^2 + |g_v| \tilde{d}_x^2 + \tilde{v}_x^2)\quad (11)$$

where $r > 1$ is chosen such that $r^2 + r g_d - g_v = 0$. This is a valid lyapunov candidate in the follower's x-axis, as it is a function of all the states, $V(0, 0) = 0$, and $V(\tilde{d}_x, \tilde{v}_x) \geq 0$.

Theorem 1: Given the Lyapunov function (11) and the estimate dynamics in (10), the estimation error \tilde{e} is globally uniformly ultimately bounded (GUUB). Furthermore, the error asymptotically converges to zero when the predecessor velocity becomes constant.

Proof. See Appendix A. \square

The numerator of the error bounds depends on the system's maximum acceleration (a_{max}), which is a physical constraint. The denominator, however, depends on the estimator gains. This indicates we can tune the estimator's behavior to achieve tighter error bounds and improve control performance.

Furthermore, Theorem 1, with a similar analysis and a corresponding Lyapunov function, establishes the GUUB property for d_y and v_y under time-varying acceleration and $\omega = 0$.

Case 3: Time-varying linear and non-zero angular velocity
We now extend our analysis to the most general scenario where the predecessor exhibits both time-varying linear velocity and non-zero angular velocity. The estimator dynamics, in this case, can be expressed as follows:

$$\dot{\tilde{e}} = \begin{bmatrix} g_d & 1 & 0 & 0 \\ g_v & 0 & 0 & 0 \\ 0 & 0 & g_d & 1 \\ 0 & 0 & g_v & 0 \end{bmatrix} \tilde{e} + \begin{bmatrix} 0 & 0 \\ -1 & 0 \\ 0 & 0 \\ 0 & -1 \end{bmatrix} \begin{bmatrix} a_x - p\omega \tilde{d}_y - \omega \tilde{v}_y \\ a_y + p\omega \tilde{d}_x + \omega \tilde{v}_x \end{bmatrix}\quad (12)$$

To analyze stability, we consider analogous Lyapunov candidates to Case 2, incorporating both x and y components:

$$V_1 = \frac{1}{2}((r\tilde{d}_x - \tilde{v}_x)^2 + |g_v|\tilde{d}_x^2 + \tilde{v}_x^2) \quad (13)$$

$$V_2 = \frac{1}{2}((r\tilde{d}_y - \tilde{v}_y)^2 + |g_v|\tilde{d}_y^2 + \tilde{v}_y^2) \quad (14)$$

$$V = V_1 + V_2 \quad (15)$$

Theorem 2: Consider the Lyapunov function $V = V_1 + V_2$ as defined in (15) and the estimator dynamics given by (12). The estimation error \tilde{e} is globally uniformly ultimately bounded (GUUB). Furthermore, when the predecessor's velocities and angular velocity converge to constants, the estimation error asymptotically converges to zero.

Proof. See Appendix B. \square

The proof of Theorem 2 highlights several important aspects of the estimator. Firstly, it confirms that the state estimation process is indeed independent of the robot's angular velocity (ω). This aligns with the expectation that a robot should be able to accurately estimate the state of other agents regardless of its own rotation. Secondly, the derived relationships between the estimator gains reveal that we can primarily tune the estimator's performance by adjusting the single parameter g_d

C. Safety-Critical Controller Design

To ensure that the followers maintain a safe distance from the predecessor, we introduce the following safety function:

$$h_1 = d_x - d_s - Tv \quad (16)$$

where d_x is the distance between the robots along the follower's x-axis, d_s is the desired safe distance, and v is the follower's linear velocity. The safe set $\mathcal{C} \subset \mathbb{R}^2$ for the safety function (16) can be defined as:

$$\mathcal{C} = \{(d_x, v) \in \mathbb{R}^2 : h_1(d_x, v) \geq 0\} \quad (17)$$

Definition 1: Given the safety set $\mathcal{C} \in \mathbb{R}^2$ defined by (17), the continuously differentiable function $h_1 : \mathbb{R}^2 \rightarrow \mathbb{R}$ in (16) is guaranteed to be in safe set \mathcal{C} if there exists an extended class \mathcal{K} function [22] denoted by α such that:

$$\dot{h}_1 \geq -\alpha(h_1) \quad (18)$$

We employ CBFs according to Definition 1 to derive a bound on the follower's acceleration that guarantees $h_1 \geq 0$, thereby maintaining safety. The derivation proceeds as follows:

$$\begin{aligned} \dot{h}_1 &= v_{1x} - v + d_y\omega - Tu \\ \dot{h}_1 &\geq -\alpha(h_1) \\ -\alpha(h_1) &\leq v_{1x} - v + d_y\omega - Tu \end{aligned} \quad (19)$$

$$Tu \leq v_{1x} - v + d_y\omega + \alpha(h_1)$$

$$Tu \leq \hat{v}_{1x} - E_u - v + d_y\omega + \alpha(h_1)$$

$$u = \kappa(\hat{v}_{1x} - E_u - x_c - v + d_y\omega + \alpha(h_1)) \quad (20)$$

where $E_u > 0$ is the upper bound on the estimation error of v_{1x} , and $x_c \geq 0$ is a constant added to achieve tracking control using the safety inequality.

To ensure the follower converges to the desired position $d_x^* + Tv$ along its axis of motion, we consider the following Lyapunov candidate:

$$V_x = 0.5(\hat{d}_x - d_x^* - Tv)^2 \quad (21)$$

To analyze the tracking dynamics, we differentiate V_x and substitute our safety-critical control law for u (20):

$$\begin{aligned} \dot{V}_x &= (\hat{d}_x - d_x^* - Tv)(\hat{v}_{1x} - v + d_y\omega + g_d\tilde{d}_x - Tu) \\ &= (\hat{d}_x - d_x^* - Tv)(E_u + x_c - \alpha(h_1) + g_d\tilde{d}_x) \\ &= (\hat{h}_1 - (d_x^* - d_s))(E_u + x_c - \alpha(\hat{h}_1 - \tilde{d}_x) + g_d\tilde{d}_x) \end{aligned} \quad (22)$$

where $\hat{h}_1 = \hat{d}_x - d_s - Tv$. We choose the class \mathcal{K} function $\alpha(h) = -g_d h$, as $g_d < 0$, $\alpha(h) > 0$ for $h > 0$, and $\alpha(0) = 0$. Substituting this definition of \hat{h}_1 and $\alpha(h)$ along with $d_e^* = d_x^* - d_s$, we obtain:

$$\begin{aligned} \dot{V}_x &= (\hat{h}_1 - d_e^*)(E_u + x_c + g_d\hat{h}_1) \\ &= (\hat{h}_1 - d_e^*)(E_u + x_c + g_d(\hat{h}_1 - d_e^*) + g_d d_e^*) \\ &= g_d(\hat{h}_1 - d_e^*)^2 + (\hat{h}_1 - d_e^*)(E_u + x_c + g_d d_e^*) \end{aligned} \quad (23)$$

This simplified derivative of V_x will be further used to prove the stability of the estimator-controller framework. To maintain a safe lateral distance between the robots, we define the safety function:

$$h_2 = \frac{d_s}{|d_s|}(d_y - d_s) \quad (24)$$

where d_y is the lateral distance and $d_s \neq 0$ is the desired safe distance. The term $\frac{d_s}{|d_s|}$ acts as a sign function, ensuring that h_2 is positive if the lateral distance $|d_y|$ exceeds the safety margin $|d_s|$, regardless of whether d_y is positive or negative.

As before, we use CBFs to derive a bound on the follower's angular velocity (ω) that guarantees $h_2 \geq 0$. The derivation proceeds as follows:

$$\dot{h}_2 = \frac{d_s}{|d_s|}(v_{1y} - d_x\omega) \quad (25)$$

$$\dot{h}_2 \geq -\alpha(h_2) \quad (26)$$

$$-\alpha(h_2) \leq \frac{d_s}{|d_s|}(v_{1y} - d_x\omega) \quad (27)$$

Choosing the same class \mathcal{K} function as longitudinal distance, for $\alpha(h) = -g_d h$, we have:

$$\begin{aligned} \frac{d_s}{|d_s|}d_x\omega &\leq \frac{d_s}{|d_s|}(v_{1y} - g_d(d_y - d_s)) \\ \frac{d_s}{|d_s|}d_x\omega &\leq \frac{d_s}{|d_s|}(\hat{v}_{1y} - g_d(d_y - d_s)) - E_\omega \\ \frac{d_s}{|d_s|}d_x\omega &= \frac{d_s}{|d_s|}(\hat{v}_{1y} - g_d(d_y - d_s)) - E_\omega - y_c \\ \omega &= \frac{\hat{v}_{1y} - g_d(d_y - d_s)}{d_x} - \frac{|d_s|(y_c + E_\omega)}{d_s d_x} \end{aligned} \quad (28)$$

The term $E_\omega > 0$ represents the upper bound on the estimation error of v_{1y} . Moreover, the term $y_c \geq 0$ is a constant added to achieve tracking control in lateral motion using the safety inequality, similar to x_c in the longitudinal motion. By calculating y_c , we ensure that the controller maintains the desired lateral distance while maintaining a safe distance.

To ensure the follower converges to the desired lateral position d_y^* , we introduce the Lyapunov candidate:

$$V_y = 0.5(\hat{d}_y - d_y^*)^2 \quad (29)$$

To analyze the tracking dynamics, we differentiate V_y and substitute our safety-critical control law for ω (28):

$$\begin{aligned} \dot{V}_y &= (\hat{d}_y - d_y^*)(\dot{v}_{1y} - d_x\omega + g_d\dot{\tilde{d}}_y) \\ &= (\hat{d}_y - d_y^*)\left(\frac{|d_s|(E_\omega + y_c)}{d_s} + g_d(d_y - d_s) + g_d\dot{\tilde{d}}_y\right) \\ &= (\hat{d}_y - d_y^*)\left(\frac{|d_s|(E_\omega + y_c)}{d_s} + g_d(\hat{d}_y - d_s)\right) \\ &= g_d(\hat{d}_y - d_y^*)^2 + (\hat{d}_y - d_y^*)\left(\frac{|d_s|(E_\omega + y_c)}{d_s} + g_d(d_y^* - d_s)\right) \end{aligned} \quad (30)$$

The final form of \dot{V}_y reveals a quadratic dependence on the lateral tracking error $(\hat{d}_y - d_y^*)$, which is a desirable property for stability analysis of the tracking controller outlined below. To establish the overall stability of our formation control scheme, we analyze two key cases: constant and time-varying predecessor velocities. For the case of constant velocity, we propose the following Lyapunov candidate function:

$$V = V_x + V_y + \tilde{e}^T P \tilde{e} \quad (31)$$

This Lyapunov function combines the individual candidates for tracking the desired distances (V_x and V_y) along with a term representing the estimation error ($\tilde{e}^T P \tilde{e}$). The positive definite matrix P is the solution to the continuous algebraic Riccati equation [21], with the state matrix A given by (III-A) and weighting matrix $Q = Q^T > 0$.

Theorem 3: Consider the Lyapunov function defined in (31), the estimator design in (4), and the controller design in (20,28). If the predecessor maintains a constant velocity (implying zero acceleration, $a_x = a_y = 0$), the distances d_x and d_y asymptotically converge to their desired values $d_x^* + Tv$ and d_y^* respectively, with $d_x^* \geq d_s - \frac{E_u}{g_d}$ and $d_y^* \geq d_s - \frac{E_\omega}{g_d}$ if $d_s > 0$, or $d_y^* \leq d_s + \frac{E_\omega}{g_d}$ if $d_s < 0$. That is, the safety distances in both longitudinal and lateral directions are maintained.

Proof. See Appendix C. \square

We now extend our analysis to the scenario where the predecessor's velocity can change over time. To establish stability in this case, we consider the following augmented Lyapunov candidate function:

$$V = V_x + V_y + V_1 + V_2 \quad (32)$$

We've added the Lyapunov candidates V_1 and V_2 from the estimator analysis (15) to the combined tracking function used in the constant velocity case.

Theorem 4: Consider the Lyapunov function defined in (31), the estimator design in (4), and the controller design in (20,28). The distances d_x and d_y asymptotically converge to their desired values $d_x^* + Tv$ and d_y^* respectively, while all the state variables of the system are guaranteed to remain globally uniformly ultimately bounded (GUUB) for $d_x^* \geq d_s - \frac{E_u}{g_d}$ and $d_y^* \geq d_s - \frac{E_\omega}{g_d}$ if $d_s > 0$ or $d_y^* \leq d_s + \frac{E_\omega}{g_d}$ if $d_s < 0$. That is,

the safety distances in both longitudinal and lateral directions are maintained.

Proof. See Appendix D. \square

The established stability properties of the proposed estimator ensure that it produces bounded estimates even when faced with sensor noise or model inaccuracies. Coupled with the proposed robust safety-critical controller design, the system gracefully handles estimation errors, maintaining its underlying safety guarantees. This resilience is essential in scenarios where sensors might fail or estimates might become temporarily unreliable.

While the current analysis focuses on an environment without friction or inertia considerations, the fundamental principles of our approach can be extended to handle more complex scenarios. By incorporating dynamic models that explicitly account for friction, drag, and inertia, we can tailor our safety-critical controllers and estimators to operate effectively in environments where these factors play a significant role. This adaptability is important for transitioning the framework to real-world applications within a wider range of dynamic settings.

IV. RESULTS AND EVALUATION

This section comprehensively evaluates the proposed estimator and control law across various formation control scenarios. The accuracy and convergence of the estimator are assessed under different conditions with zero and non-zero angular velocity. The system's behavior in a basic formation scenario is examined through a simulation of a four-agent system arranged in a diamond formation (as illustrated in Fig. 1), with the leader maintaining a constant velocity. This simulation allows observation of how the agents coordinate their movements and maintain the desired formation while adhering to safety constraints. String stability, a critical factor in the robustness of multi-agent systems, is thoroughly analyzed by examining the propagation of disturbances through the formation. This analysis provides valuable insights into how well the follower agents can mitigate the effects of disturbances from the leader and ensure the formation's overall stability. The evaluation extends beyond simulations in Python by conducting experiments in the physics engine-based Gazebo simulation environment. A three-agent system arranged in a triangular formation is simulated, introducing realistic physics and sensor noise into the scenario. This simulation offers a more comprehensive and practical assessment of the system's performance, as it is exposed to challenges typically encountered in real-world applications.

For scenarios involving zero and non-zero angular velocity, the four-agent diamond formation with constant leader velocity, and the string stability analysis, the system's continuous-time behavior is simulated using the 4th-order Runge-Kutta method. The distance sensor data for each vehicle is simulated using the difference in states between vehicles. Throughout these simulations, the agent's linear velocity, acceleration, and angular velocity are bounded to 1 m/s, 0.5 m/s², and 2 rad/s, respectively. The gain used for the estimator is $g_d = -15$, and the remaining parameters are calculated as $g_v = -50$, $p = -5$, $r = 10$, $T = 0.2sec$ and $k_d = 725$. The safety bounds

for the controller, E_u and E_ω , are both set to 1.4. For this choice of gains, the state matrix A exhibited Hurwitz properties for $\omega = 0$, characterized by eigenvalues of $[-5, -5, -10, -10]$, ensuring stability.

A. Estimator Analysis

This subsection evaluates the performance of the proposed estimator under varying conditions. A two-agent system is simulated, where both agents accelerate for two seconds to a fixed linear velocity of 0.2 m/s. Agent 1 maintains a constant angular velocity of 0.2 rad/s, while Agent 2 has zero angular velocity. This setup enables the evaluation of three distinct scenarios: a) estimating the state of the accelerating agent while accelerating, in which Agent 1 estimates the state of Agent 2 during the initial acceleration phase (0-2 seconds); b) estimating the state of an agent with constant linear velocity while moving with non-zero angular velocity, in which Agent 1 estimates the state of Agent 2 after the 2-sec acceleration phase, where Agent 2 is moving at a constant velocity while Agent 1 maintains its angular velocity; and c) estimating the state of an agent with non-zero angular velocity while moving with zero angular velocity, in which Agent 2 estimates the state of Agent 1 after the 2-sec acceleration phase, where Agent 1 is moving at a constant velocity with non-zero angular velocity while Agent 2 remains stationary in terms of angular motion.

During the first scenario, the initial acceleration phase (0-2 seconds), both agents are accelerating at 0.2 m/s^2 . In line with Case 3 in Section III-B, the estimator is expected to exhibit GUUB behavior. The theoretical bounds for the position and velocity errors are approximately $\pm\sqrt{c_i/k_d} = \pm 0.026 \text{ m}$ and $\pm(|r\dot{d}_x + \sqrt{c_i/(r-1)}) = 0.497 \text{ m/s}$, respectively. Numerical simulation results in Fig. 3 show the position error converging to 0.004 m and the velocity error to 0.06 m/s, both well within the expected bounds.

After the acceleration phase in the second scenario, Agent 2 moves at a constant velocity while Agent 1 maintains angular motion. As the estimator's convergence is theoretically independent of the observer's angular velocity, the estimation errors are anticipated to approach zero. Simulation results in Fig. 3 confirm this, with the distance error converging to 0.0003 m and the velocity error to 0.00004 m/s.

Finally, in the third scenario, Agent 1 moves with constant linear and angular velocity, while Agent 2 remains stationary in terms of angular motion. The estimator effectively perceives the angular motion as an additional acceleration ($a = u + v\omega = 0.08 \text{ m/s}^2$). Therefore, the estimation errors are expected to be GUUB, with bounds similar to those in the first scenario (acceleration with estimation). The simulated results in Fig. 3 corroborate this, showing convergence of the distance error to 0.0018 m and the velocity error to 0.0004 m/s.

B. Formation control with constant leader velocity

This section evaluates the proposed control framework under the condition of constant leader velocity. The leader agent accelerates to achieve a constant linear velocity while maintaining a constant angular velocity of $\omega = 0.5 \text{ rad/s}$. This configuration steers the leader along a circular trajectory,

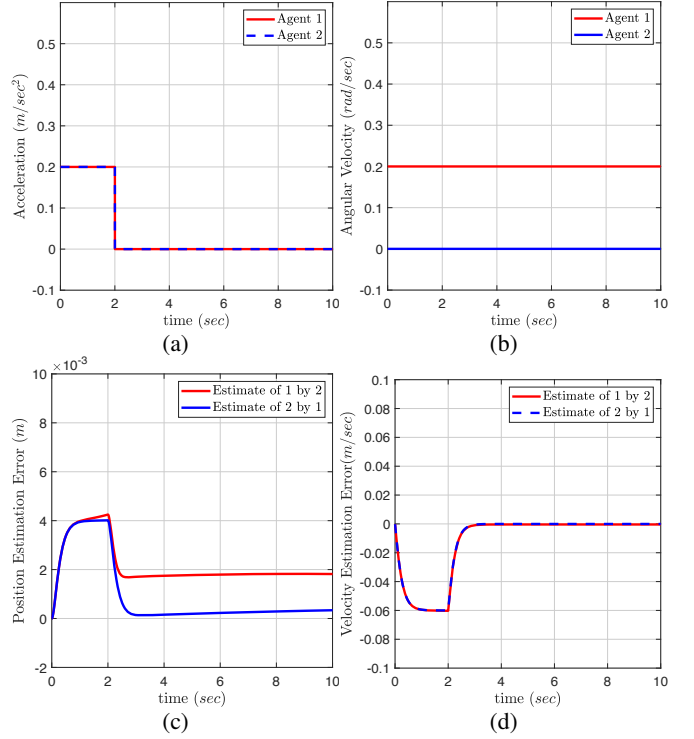


Fig. 3. Estimator performance for a two-agent system with different control profiles: (a) Linear acceleration profiles; (b) Angular velocities; (c) Position estimation errors; (d) Velocity estimation errors.

a common benchmark in formation control studies. Notably, due to the non-zero angular velocity (ω), the acceleration components a_x and a_y are non-zero, classifying this scenario under the time-varying stability analysis detailed in *Theorem 4*.

Fig. 4 (a, b, c) illustrates the linear velocity, acceleration, and angular velocity profiles of each agent throughout the experiment. The plots demonstrate rapid convergence to a circular formation that mirrors the leader's trajectory. Angular velocities converge to the leader's value, while linear velocities converge to values determined by each agent's respective radius of circular motion. Notably, this orchestrated behavior is achieved solely through the proposed framework, showcasing the estimator-controller's capability to execute maneuvers commonly explored in formation control without any controller modifications.

The safety region for each agent is defined as 0.3 m, with a desired separation of 0.1 m between each follower. Fig. 4 (d, e) shows the evolution of safety control barrier functions along and perpendicular to the agents' motion. Despite the desired separation falling within an unsafe region, the agents consistently adhere to safety constraints, maintaining a minimum conservative distance. Fig. 4 (f) visually presents the agent's motion during the experiment.

C. String Stability Performance

String stability is a critical performance metric for leader-follower systems. It ensures that disturbances like sudden braking or acceleration do not propagate to the followers, causing potential collisions. In a string-stable formation control design, the amplitude of sinusoidal velocity disturbances

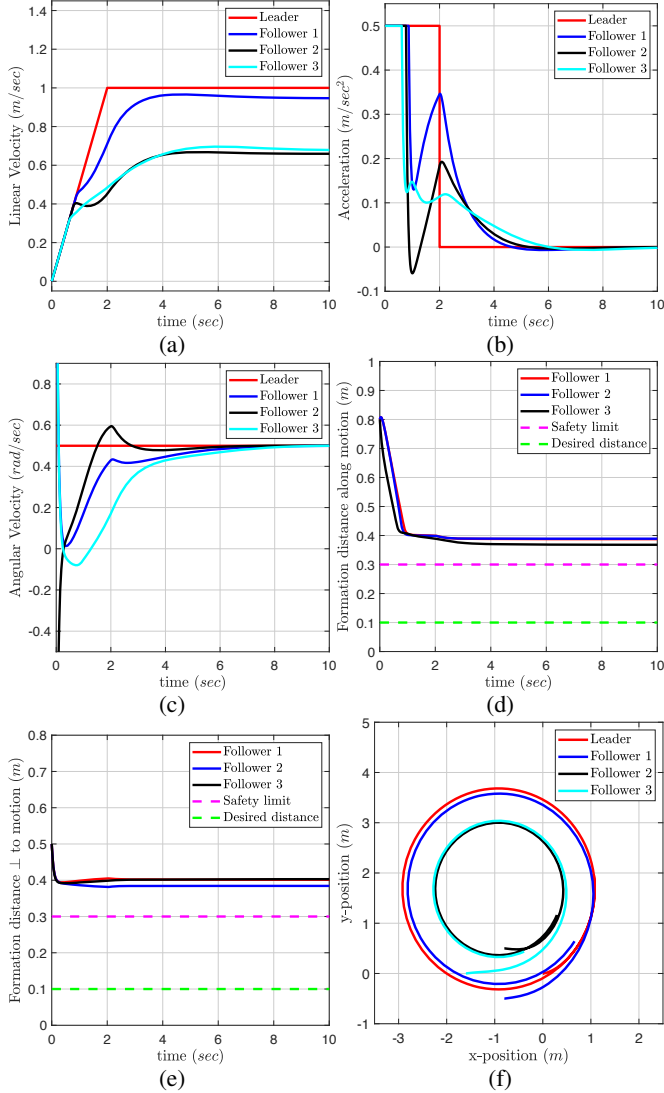


Fig. 4. Formation control for a circular motion using the proposed framework: (a) Linear velocity profiles; (b) Acceleration profiles; (c) Angular velocities; (d) distances maintained along the motion; (e) Position estimation errors; (e) Distance perpendicular to the motion, and (f) Overall motion of the formation.

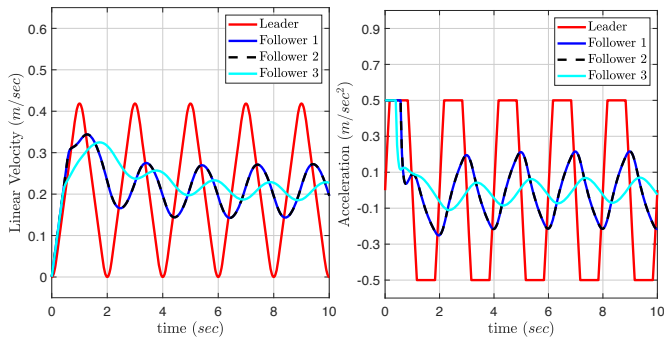


Fig. 5. Disturbance attenuation in linear velocity and acceleration for a 4-agent diamond formation control. Left: linear velocity disturbance of 0.415 m/s. Right: acceleration disturbance of 1.0 m/s².

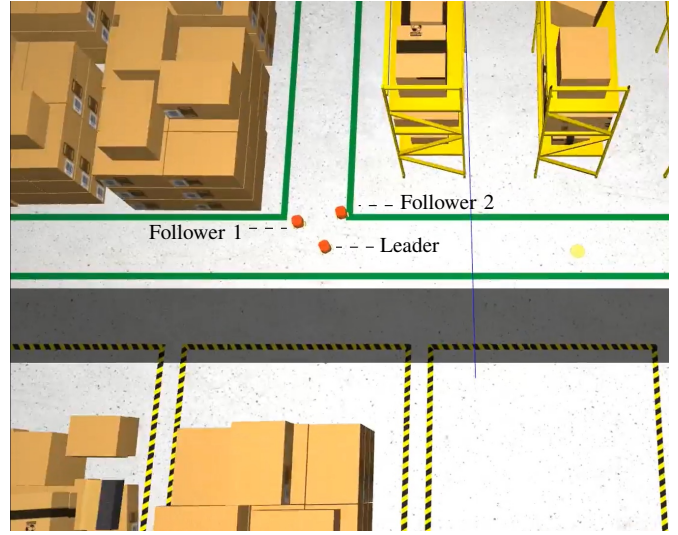


Fig. 6. Snapshot of the warehouse environment in Gazebo with three Turtlebot3 in a triangular formation.

should decrease from the leader to the end of the platoon. Fig. 5 illustrates the performance of the proposed controller in maintaining string stability for the considered formation.

In this experiment, the leader's velocity underwent a disturbance with an amplitude of 0.415 m/s. As the disturbance propagated through the formation, the resulting amplitudes diminished to 0.12 m/s for both follower 1 and follower 2 and further to 0.035 m/s for follower 3, as shown in Fig. 5 (a). Similarly, for an acceleration disturbance of 1.0 m/s², the proposed framework calculated accelerations of 0.434 m/s² for both follower 1 and follower 2 and 0.14 m/s² for follower 3, as shown in Fig. 5 (b). Notably, the identical states of follower 1 and follower 2, along with their pursuit of the same predecessor, resulted in overlapping velocity and acceleration profiles. The quantitative outcomes reveal an average string stability gain (S) of 0.29. The observed decrease in amplitude of linear velocity and acceleration profiles towards the end of the platoon, coupled with $S < 1$, confirms the string stability of the proposed control law.

D. Physics Engine-Based Experiments

To comprehensively assess the feasibility and effectiveness of the proposed estimation-based controller within real-world scenarios, we evaluate the framework using the Gazebo simulation environment. This section presents the dynamic evolution of system states and estimator errors for a triangular formation control operating under the proposed framework. The experimental setup entailed a leader agent navigating along a time-varying trajectory within a simulated warehouse environment and two followers following the leader to maintain the triangular formation, employing Turtlebot3 models for the robots within the Gazebo framework. Key parameters governing robot behavior, including maximum linear velocity, angular velocity, and acceleration, were set at 0.3 m/s, 1.0 rad/s, and 1.0 m/s², respectively. A snapshot of the warehouse environment in the Gazebo simulation from the experiment with the Turtlebot3 models is depicted in Fig. 6.

A three-agent cluster operating without inter-vehicle communication is analyzed. Within this setup, the leader agent exhibited variable velocity while the two follower agents autonomously maintained formation relative to the leader under the purview of the proposed controller. Initially, follower 1 and follower 2 are positioned at coordinates $(-0.5, -0.4)$ and $(-0.5, 0.4)$ relative to the leader, respectively. Distance sensors are emulated in software, considering the differences between agent states. The controller and estimator are parameterized with values of $g_d = -6$, $g_v = -8$, $p = -2$, $E_\omega = 0.4$ m-rad/s, $E_u = 0.4$ m/s, and $T = 0.2$ sec, ensuring the robustness and adaptability of the system across varying scenarios. The state matrix A exhibited Hurwitz properties for $\omega = 0$, characterized by eigenvalues of $[-2, -2, -4, -4]$, ensuring stability within the system dynamics. Safety parameters are set to maintain a 0.2 m safe distance in all directions. Follower 1 and follower 2 are assigned formation parameters to maintain distances of 0.4 m longitudinally and 0.3 m laterally, and 0.4 m longitudinally and -0.3 m laterally from the leader, respectively.

The leader agent's time-varying trajectory is determined by the angular velocity and acceleration curves shown in Fig. 7 (a, b). These plots demonstrate that the proposed controller generates acceleration and angular velocity commands to maintain the desired triangular formation. This is further confirmed by Fig. 7 (c), which showcases the evolution of the agents' linear velocities. When the leader operates with zero angular velocity, the linear velocities of follower 1 and follower 2 converge to the leader's linear velocity. Conversely, when the leader initiates rotation around a center of rotation, the follower closer to the center reduces its speed, while the follower farther from the center increases its speed to maintain formation integrity. Notably, the angular velocities of all agents remain synchronized to maintain formation, as verified in Fig. 7 (a). Fig. 7 (d, e) illustrates the convergence of formation distances to their desired values when the leader agent's acceleration and angular velocity are zero. In scenarios with non-zero angular velocity, the deviations between the formation distance and the desired distance remain bounded within 0.02 m along the motion and 0.005 m perpendicular to the motion. Importantly, both follower agents consistently adhere to the predefined safety limits throughout the experiment. Fig. 7 (f) visually represents the trajectories of the leader and follower agents.

The stability of the estimator within the Gazebo environment is essential for the optimal performance of the proposed framework. Fig. 8 illustrates the estimation errors in the position and velocity of the leader as perceived by the follower agents. While some noisy spikes are observed, the position estimation error remains less than 0.002 m when the leader agent has zero angular velocity. For cases with non-zero leader angular velocity, the position estimation errors for both followers are bounded within 0.004 m. Furthermore, the velocity estimation errors for both follower agents remain below 0.006 m/s. This demonstrates the estimator's robustness to noise in real-world environments.

Videos of the experiment presented in this section can be found in the accompanying video for the article, available at <https://vimeo.com/958141327/9fb69cf6cc>

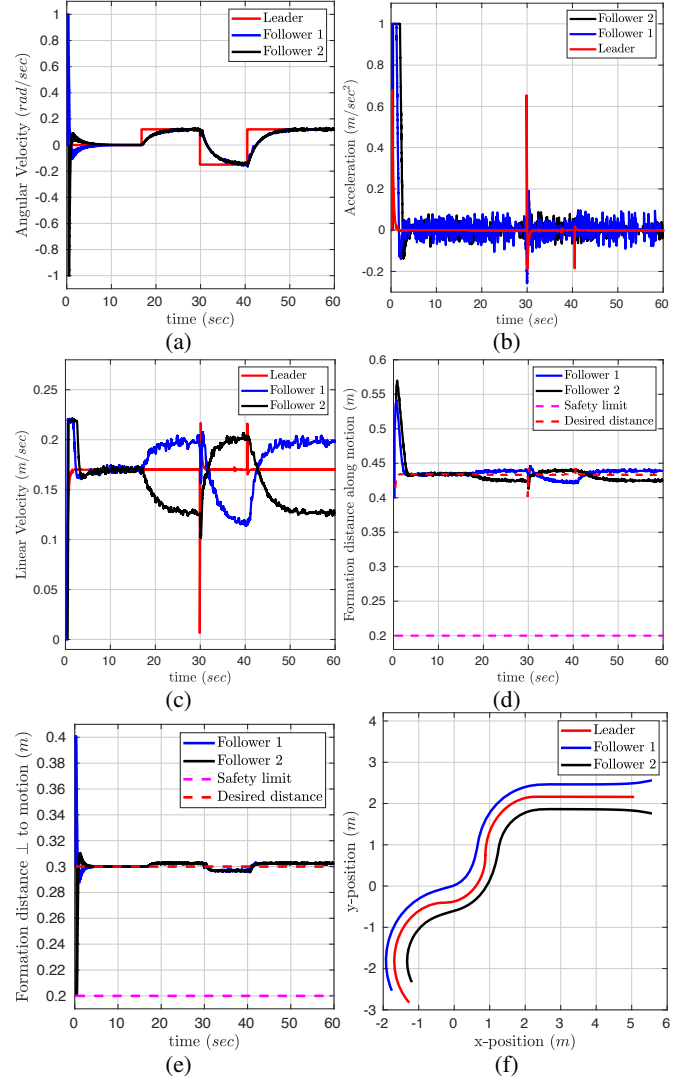


Fig. 7. Plots for formation control of triangular formation in Gazebo environment using the proposed framework: (a) Angular Velocity, (b) Acceleration, (c) Linear Velocity, (d) Distance along the motion, (e) Distance perpendicular to the motion, and (f) Overall motion of the formation.

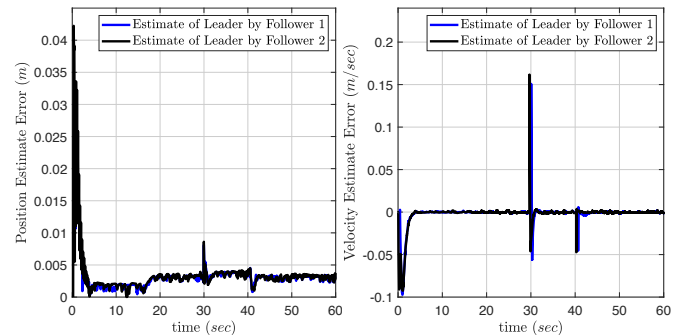


Fig. 8. Leader's position (left) and velocity (right) estimation error when estimated by follower agents.

The results obtained from the Gazebo simulation experiments substantiate the applicability and effectiveness of the proposed controller in real-world scenarios. The comprehensive evaluation demonstrates its ability to maintain safety-critical performance while achieving the desired formation control.

V. CONCLUSIONS AND FUTURE WORK

This research addresses the critical challenge of achieving stable and safe formation control for non-holonomic mobile robots in environments where communication is constrained or unreliable. We have presented a novel estimator-based safety-critical controller framework that successfully addresses the challenge of the absence of inter-robot communication while maintaining a safe distance between agents. The proposed estimator, designed for non-holonomic robot swarms, demonstrates robustness and stability even under challenging conditions of time-varying predecessor velocities and angular velocities. Our theoretical analysis, based on Lyapunov theory, establishes the stability of the estimation errors, guaranteeing the estimator's reliability. The safety-critical controller, integrated with the estimator, utilizes CBFs to ensure inter-agent safety at all times, preventing collisions even when the desired formation configuration involves close proximity between agents. By utilizing the concept of string stability in the context of leader-follower formation control, we demonstrated that the proposed controller effectively attenuates disturbances propagating through the formation. Our comprehensive evaluation, including numerical simulations and Gazebo experiments with realistic physics and sensor noise, validates the effectiveness of the proposed framework. The estimator demonstrates robustness in the face of noise, with position errors bounded within acceptable limits, and the controller successfully guides the formation while adhering to safety constraints.

This research lays a foundation for safe and reliable formation control in a wide range of applications where communication constraints and sensor limitations are prevalent. Future work will focus on including dynamic reconfiguration of the formation while maintaining safety and stability, extending the framework to accommodate more complex robot dynamics or heterogeneous multi-robot systems, and incorporating additional safety considerations such as obstacle avoidance.

APPENDIX A PROOF OF THEOREM 1

We analyze the stability properties of the estimator by examining the time derivative of the Lyapunov function V :

$$\begin{aligned}\dot{V} &= (r\tilde{d}_x - \tilde{v}_x)(rg_d\tilde{d}_x + r\tilde{v}_x - g_v\tilde{d}_x + a_x) \\ &\quad + |g_v|\tilde{d}_x(g_d\tilde{d}_x + \tilde{v}_x) + \tilde{v}_x(g_v\tilde{d}_x - a_x) \\ &= (r\tilde{d}_x - \tilde{v}_x)(-r^2\tilde{d}_x + r\tilde{v}_x + a_x) + |g_v|g_d\tilde{d}_x^2 - \tilde{v}_x a_x \\ &= -r(r\tilde{d}_x - \tilde{v}_x)^2 + (r\tilde{d}_x - \tilde{v}_x)a_x + |g_v|g_d\tilde{d}_x^2 - \tilde{v}_x a_x \\ &= -r(r\tilde{d}_x - \tilde{v}_x)^2 + 2(r\tilde{d}_x - \tilde{v}_x)a_x + |g_v|g_d\tilde{d}_x^2 - r\tilde{d}_x a_x \\ &= (1-r)(r\tilde{d}_x - \tilde{v}_x)^2 + (|g_v|g_d + \frac{r^2}{4})\tilde{d}_x^2 \\ &\quad - (r\tilde{d}_x - \tilde{v}_x - a_x)^2 - (\frac{r}{2}\tilde{d}_x - a_x)^2 + 2a_x^2\end{aligned}\quad (33)$$

Applying the physical constraint on the magnitude of acceleration, $|a_x| < a_{max}$, we obtain:

$$\begin{aligned}\dot{V} &\leq (1-r)(r\tilde{d}_x - \tilde{v}_x)^2 + (|g_v|g_d + \frac{r^2}{4})\tilde{d}_x^2 \\ &\quad - (|r\tilde{d}_x - \tilde{v}_x| - a_{max})^2 - (|\frac{r}{2}\tilde{d}_x| - a_{max})^2 + 2a_{max}^2\end{aligned}\quad (34)$$

Defining $c_i = 2a_{max}^2$, and considering the expression for \dot{V} , we conclude $\dot{V} < 0$ (indicating stability) as long as one of the following conditions holds:

$$|\tilde{d}_x| > \epsilon_d \doteq \min\left(\frac{2(\sqrt{c_i} + a_{max})}{r}, \sqrt{\frac{c_i}{k_d}}\right)\quad (35)$$

where $k_d = -(|g_v|g_d + \frac{r^2}{4})$, or

$$|r\tilde{d}_x - \tilde{v}_x| > \epsilon_v \doteq \min\left(\sqrt{c_i} + a_{max}, \sqrt{\frac{c_i}{r-1}}\right)\quad (36)$$

where ϵ_d and ϵ_v represent bounds on the estimation errors in d_x and v_x respectively.

Invoking an extension of Lyapunov's theorem, we establish the estimator's global stability and the GUUB property of d_x and v_x .

APPENDIX B PROOF OF THEOREM 2

Following a similar calculation to Theorem 1, we obtain expressions for the time derivatives of V_1 and V_2 :

$$\begin{aligned}\dot{V}_1 &= -r(r\tilde{d}_x - \tilde{v}_x)^2 + |g_v|g_d\tilde{d}_x^2 \\ &\quad + (r\tilde{d}_x - 2\tilde{v}_x)(a_x - p\omega\tilde{d}_y - \omega\tilde{v}_y)\end{aligned}\quad (37)$$

$$\begin{aligned}\dot{V}_2 &= -r(r\tilde{d}_y - \tilde{v}_y)^2 + |g_v|g_d\tilde{d}_y^2 \\ &\quad + (r\tilde{d}_y - 2\tilde{v}_y)(a_y + p\omega\tilde{d}_x + \omega\tilde{v}_x)\end{aligned}\quad (38)$$

Substituting $r = -2p$ into these expressions, we arrive at a simplified expression for the time derivative of the combined Lyapunov function, $\dot{V} = \dot{V}_1 + \dot{V}_2$:

$$\begin{aligned} \dot{V} &= -r(r\tilde{d}_x - \tilde{v}_x)^2 + |g_v|g_d(\tilde{d}_x^2 + \tilde{d}_y^2) - r(r\tilde{d}_y - \tilde{v}_y)^2 \\ &\quad + (r\tilde{d}_x - 2\tilde{v}_x)a_x + (r\tilde{d}_y - 2\tilde{v}_y)a_y \\ &= (1-r)((r\tilde{d}_x - \tilde{v}_x)^2 + (r\tilde{d}_y - \tilde{v}_y)^2) + k_d(\tilde{d}_x^2 + \tilde{d}_y^2) \\ &\quad - (r\tilde{d}_x - \tilde{v}_x - a_x)^2 - \left(\frac{r}{2}\tilde{d}_x - a_x\right)^2 + 2a_x^2 \\ &\quad - (r\tilde{d}_y - \tilde{v}_y - a_y)^2 - \left(\frac{r}{2}\tilde{d}_y - a_y\right)^2 + 2a_y^2 \end{aligned} \quad (39)$$

Incorporating the physical constraint on the magnitude of the predecessor's acceleration $a_x^2 + a_y^2 < a_{max}^2$, we complete the square to obtain an expression for \dot{V} .

$$\begin{aligned} \dot{V} &\leq (1-r)((r\tilde{d}_x - \tilde{v}_x)^2 + (r\tilde{d}_y - \tilde{v}_y)^2) + k_d(\tilde{d}_x^2 + \tilde{d}_y^2) \\ &\quad - (|r\tilde{d}_x - \tilde{v}_x| - a_{max})^2 - \left(\frac{r}{2}\tilde{d}_x - a_{max}\right)^2 \\ &\quad - (|r\tilde{d}_y - \tilde{v}_y| - a_{max})^2 - \left(\frac{r}{2}\tilde{d}_y - a_{max}\right)^2 + 2a_{max}^2 \end{aligned} \quad (40)$$

By carefully analyzing the form of \dot{V} , we derive conditions under which it is strictly negative. These conditions translate into bounds on the estimation errors \tilde{d}_x , \tilde{d}_y , \tilde{v}_x , and \tilde{v}_y , demonstrating the GUUB property of the estimator.

Exploiting the constraint $r^2 + rg_d - g_v = 0$ and the substitution $r = -2p$, we obtain an explicit relationship between the estimator gains g_d and g_v :

$$p = \frac{g_d}{3} \quad \text{and} \quad g_v = \frac{-2g_d^2}{9} \quad (41)$$

This indicates that the estimator behavior can be tuned primarily through the choice of g_d .

APPENDIX C PROOF OF THEOREM 3

Recall our Lyapunov function V in (31). Differentiating V and substituting the expressions for \dot{V}_x , \dot{V}_y , and the estimator dynamics, we obtain:

$$\begin{aligned} \dot{V} &= \dot{V}_x + \dot{V}_y + \tilde{e}^T(A^T P + PA)\tilde{e} \\ &= g_d(\hat{h}_1 - d_e^*)^2 + (\hat{h}_1 - d_e^*)(E_u + x_c + g_d d_e^*) \\ &\quad - \tilde{e}^T Q \tilde{e} + g_d(\hat{d}_y - d_y^*)^2 \\ &\quad + (\hat{d}_y - d_y^*)\left(\frac{|d_s|(E_\omega + y_c)}{d_s} + g_d(d_y^* - d_s)\right) \end{aligned} \quad (42)$$

We strategically substitute for x_c and y_c using the provided conditions on d_x^* and d_y^* . As $x_c \geq 0$ and $d_x^* \geq d_s - \frac{E_u}{g_d}$, we can substitute the constant x_c as $x_c = -g_d(d_x^* - d_s) - E_u$. Similarly, as $y_c \geq 0$, we can substitute the constant y_c as $y_c = \frac{|d_s|}{d_s}(-g_d(d_y^* - d_s)) - E_\omega$. Note that the quadratic terms in \dot{V} have a coefficient g_d , which is negative by design. Similarly, the matrix Q in the estimator term is positive definite. This gives:

$$\dot{V} = g_d(\hat{h}_1 - d_e^*)^2 - \tilde{e}^T Q \tilde{e} + g_d(\hat{d}_y - d_y^*)^2 \quad (43)$$

Consequently, \dot{V} is negative definite, indicating stability according to Lyapunov's theorem. As $g_d < 0$ and $Q < 0$, d_x and d_y are proven to converge to $d_x^* + Tv$ and d_y^* respectively. This implies that the tracking errors in both d_x and d_y asymptotically converge to zero, achieving our desired formation configuration.

APPENDIX D PROOF OF THEOREM 4

Detailed calculations, leveraging the results from Theorems 2 and 3, allow us to derive an upper bound on the time derivative of the augmented Lyapunov function in (32), i.e. \dot{V} . By applying the physical constraints on acceleration and manipulating the expression for \dot{V} , we establish conditions under which \dot{V} is strictly negative:

$$\begin{aligned} \dot{V} &\leq (1-r)((r\tilde{d}_x - \tilde{v}_x)^2 + (r\tilde{d}_y - \tilde{v}_y)^2) + k_d(\tilde{d}_x^2 + \tilde{d}_y^2) \\ &\quad - (|r\tilde{d}_x - \tilde{v}_x| - a_{max})^2 - \left(\frac{r}{2}\tilde{d}_x - a_{max}\right)^2 \\ &\quad - (|r\tilde{d}_y - \tilde{v}_y| - a_{max})^2 - \left(\frac{r}{2}\tilde{d}_y - a_{max}\right)^2 \\ &\quad + g_d(\hat{h}_1 - d_e^*)^2 + g_d(\hat{d}_y - d_y^*)^2 + 2a_{max}^2 \end{aligned}$$

For $c_i = 2a_{max}^2$, we can conclude that $\dot{V} < 0$ as long as either

$$|\hat{d}_x - d_x^* - Tv| > \epsilon_x \doteq \sqrt{\frac{c_i}{|g_d|}} \quad (44)$$

or,

$$|\hat{d}_y - d_y^*| > \epsilon_y \doteq \sqrt{\frac{c_i}{|g_d|}} \quad (45)$$

is satisfied. These conditions translate into explicit bounds on the formation errors in both the longitudinal (ϵ_x) and lateral (ϵ_y) directions.

Invoking an extension of Lyapunov's theorem, we conclude that both the estimator states and the formation states exhibit the global uniform ultimate boundedness (GUUB) property. This guarantees that all system states will remain within well-defined regions. Furthermore, by combining the derived tracking error bounds with the bounds on estimation errors established in our estimator analysis, we obtain explicit expressions for the maximum allowable deviations of the distances d_x and d_y from their desired values:

$$|d_x - d_x^* - Tv| < \epsilon_x + \epsilon_d \quad (46)$$

$$|d_y - d_y^*| < \epsilon_y + \epsilon_d \quad (47)$$

REFERENCES

- [1] R. N. Darmanin and M. K. Bugeja, "A review on multi-robot systems categorised by application domain," in *2017 25th Mediterranean Conference on Control and Automation (MED)*, 2017, pp. 701–706.
- [2] K.-K. Oh, M.-C. Park, and H.-S. Ahn, "A survey of multi-agent formation control," *Automatica*, vol. 53, pp. 424–440, 2015.
- [3] J. Lin, Y. Wang, Z. Miao, Q. Lin, G. Hu, and R. Fierro, "Robust linear-velocity-free formation tracking of multiple quadrotors with unknown disturbances," *IEEE Transactions on Control of Network Systems*, vol. 10, no. 4, pp. 1757–1769, 2023.
- [4] P. Aditya, E. Apriliani, G. Zhai, and D. K. Arif, "Formation control of multi-robot motion systems and state estimation using extended kalman filter," in *2019 International Conference on Electrical Engineering and Informatics (ICEEI)*. IEEE, 2019, pp. 99–104.

- [5] S. Moorthy and Y. H. Joo, "Formation control and tracking of mobile robots using distributed estimators and a biologically inspired approach," *Journal of Electrical Engineering & Technology*, vol. 18, no. 3, pp. 2231–2244, 2023.
- [6] S. Zhu, K. Lv, Z. Yang, C. Chen, and X. Guan, "Bearing-based formation tracking control of nonholonomic mobile agents with a persistently exciting leader," *IEEE Transactions on Control of Network Systems*, vol. 11, no. 1, pp. 307–318, 2024.
- [7] J. Zhao, K. Zhu, H. Hu, X. Yu, X. Li, and H. Wang, "Formation control of networked mobile robots with unknown reference orientation," *IEEE/ASME Transactions on Mechatronics*, vol. 28, no. 4, pp. 2200–2212, 2023.
- [8] A. D. Ames, S. Coogan, M. Egerstedt, G. Notomista, K. Sreenath, and P. Tabuada, "Control barrier functions: Theory and applications," in *2019 18th European Control Conference (ECC)*, 2019, pp. 3420–3431.
- [9] B. A. Butler, C. H. Leung, and P. E. Paré, "Collaborative safe formation control for coupled multi-agent systems," *arXiv preprint arXiv:2311.11156*, 2023.
- [10] A. Rai and S. Mou, "Safe region multi-agent formation control with velocity tracking," *Systems & Control Letters*, vol. 186, p. 105776, 2024.
- [11] B. Yan, P. Shi, C. P. Lim, Y. Sun, and R. K. Agarwal, "Security and safety-critical learning-based collaborative control for multiagent systems," *IEEE Transactions on Neural Networks and Learning Systems*, pp. 1–12, 2024.
- [12] Y. Sun, D. Wu, L. Gao, Y. Gao, Y. Pan, and N. Ding, "Safety-critical control and path following by formations of agents with control barrier functions using distributed model predictive control," in *2023 35th Chinese Control and Decision Conference (CCDC)*, 2023, pp. 1818–1823.
- [13] R. Rahimi, F. Abdollahi, and K. Naqshi, "Time-varying formation control of a collaborative heterogeneous multi agent system," *Robotics and autonomous systems*, vol. 62, no. 12, pp. 1799–1805, 2014.
- [14] V. P. Tran, M. Garratt, and I. R. Petersen, "Switching time-invariant formation control of a collaborative multi-agent system using negative imaginary systems theory," *Control Engineering Practice*, vol. 95, p. 104245, Feb. 2020.
- [15] H. Li, J. Hu, Q. Zhou, and B. K. Ghosh, "Safe formation control of multiple unmanned aerial vehicles: control design and safety-stability analysis," *Control Theory and Technology*, pp. 1–13, 2024.
- [16] X. Liang, H. Wang, Y.-H. Liu, Z. Liu, and W. Chen, "Leader-following formation control of nonholonomic mobile robots with velocity observers," *IEEE/ASME Transactions on Mechatronics*, vol. 25, no. 4, pp. 1747–1755, 2020.
- [17] Y. Hong, G. Chen, and L. Bushnell, "Distributed observers design for leader-following control of multi-agent networks (extended version)," *arXiv preprint arXiv:1801.00258*, 2017.
- [18] L. Wang, J. Xi, M. He, and G. Liu, "Robust time-varying formation design for multiagent systems with disturbances: Extended-state-observer method," *International Journal of Robust and Nonlinear Control*, vol. 30, no. 7, p. 2796–2808, Mar. 2020.
- [19] V. Bohara and S. Farzan, "Adaptive estimation-based safety-critical cruise control of vehicular platoons," *IEEE Transactions on Vehicular Technology*, pp. 1–13, 2024.
- [20] G. Orosz, "Connected cruise control: modelling, delay effects, and nonlinear behaviour," *Vehicle System Dynamics*, vol. 54, no. 8, pp. 1147–1176, 2016.
- [21] P. L. L. Rodman, *Algebraic Riccati equations*, 2nd ed. Oxford University Press, 1995.
- [22] H. K. Khalil, *Nonlinear systems*, 2nd ed. Upper Saddle River, NJ 07458: Prentice-Hall, 2011.